Supplementary Information

Supplementary methods

Modeling for the recruitment of the next chaperone:subunit FimC:FimA complex in assembly by the FimD:FimC:FimF:FimG:FimH complex. In the modeling exercise presented in Fig. 1B, 3BWU and 4DWH are first superposed using FimC, yielding a model of FimC:FimA bound to the NTD of FimD. This model is then superposed to the FimD:tip complex using FimD NTD, yielding a model of the FimD:FimC:FimF:FimG:FimH:FimC':FimA complex where FimC':FimA is bound to the NTD of FimD.

Supplementary Table 1. Data collection and refinement statistics

The FimD:FimC:FimF:FimG:FimH structure was refined to 4.3, 4.1, and 3.8 Å resolutions. Step-wise extension of the resolution to 3.8 Å resulted in an improved structural model as indicated by lower Rfree values in the pair-wise refinement procedure described by Karplus and Diederichs (2012)[1] (see Supplementary Table 2), lower Molprobity scores (this table), and improved electron density (see Supplementary Fig. 4).

FimD:FimC:FimF:FimG:FimH			
Data collection			
Space group	$P4_22_12$	$P4_22_12$	$P4_22_12$
Cell dimensions			
a, b, c (Å)	122.36,122.36,328.46	122.36,122.36,328.46	122.36,122.36,328.46
α, β, γ (°)	90, 90, 90	90, 90, 90	90, 90, 90
Resolution (Å)	83.67 - 3.8	83.67 – 4.1	83.67 – 4.3
R_{sym} (%) [a]	13.6 (409.6)	10.4 (189.8)	8.9 (96.6)
$CC_{1/2}$; pairs	99.9 (18.4); n=1862	99.9 (60.9); n=1387	100 (80.4); n=1163
I/σI	13.73 (0.52)	17.04 (1.24)	19.41 (2.43)
Completeness (%)	99.84 (99.96)	99.80 (100)	99.80 (100)
Total reflections	241355	194064	168023
Unique reflections	25474	20402	17762
Multiplicity	9.47 (8.65)	9.49 (9.87)	9.44 (9.78)
Refinement			
Resolution (Å)	83.67 - 3.8	83.67 – 4.1	83.67 – 4.3
R_{work}/R_{free} [b, c]	24.80/29.76	23.81/28.95	23.23/28.70
No. atoms	11733	11733	11733
Ligand/ion	0	0	0
Water	0	0	0
B-factors (Å^2)			
Wilson B	191.7	190.3	186.14
Protein	194.37	192.25	192.67
R.m.s deviations			
Bond lengths (Å)	0.002	0.002	0.002
Bond angles (°)	0.45	0.44	0.45
Ramachandran			
favored (%)	91.0	91.0	91.0
outliers (%)	0.8	0.8	0.8
Molprobity			
Clashscore	10.1	10.43	10.56
Overall score	2.47	2.48	2.49

[a] $R_{sym} = \Sigma|I - \langle I\rangle|/\Sigma\langle I\rangle$, where I is the observed and $\langle I\rangle$ is the average intensity of the given reflection.

[b] $R_{work} = \Sigma_{hkl} ||F_{obs}| - |F_{calc}|| / \Sigma_{hkl} |F_{obs}|$.

[c] R_{free} is defined as above but calculated for 5% of reflections randomly excluded from the refinement.

Numbers in parentheses are for the highest resolution shell (3.9 – 3.8 Å, 4.2 – 4.1 Å, 4.4 – 4.3 Å for the 3.8, 4.1, and 4.3 Å resolution structures).

Supplementary Table 2. Pair-wise refinement of the FimD:FimC:FimF:FimG:FimH complex structure.

		High-resolution limit for refinement (Å)			
		4.1	**4.0**	**3.9**	**3.8**
High-resolution limit for R/Rfree values calculation (Å)	**4.1**	23.81/28.95	23.85/28.89		
	4.0		24.13/29.14	24.04/29.10	
	3.9			24.29/29.48	24.48/29.41
	3.8				24.80/29.76

The procedure is described in Karplus and Diederichs (2012)[1]. In brief, the structural model is refined step-wise by increasing the resolution by intervals of 0.1 Å. In each step, once the model is refined to a given resolution, the resulting model is used to calculate the R and Rfree values at the lower resolution of the previous refinement cycle without refining this model again. Here, a model refined to a Rfree of 28.95 at a resolution of 4.1 Å served as the starting model. Refinement was then carried out to 4.0 Å to a Rfree of 29.14, and this 4.0 Å resolution refined model was used to calculate R and Rfree values using the 4.1 Å resolution data, yielding a Rfree of 28.89. This is lower than the 28.95 Rfree value obtained with the original model at this resolution, indicating that the model refined at 4.0 Å resolution is of slightly better quality than that at 4.1 Å. The same protocol was used to progressively include higher resolution data, first to 3.9 Å and then 3.8 Å resolution. As can be seen, there is steady improvement of the Rfree value when compared to the previous refinement cycle, indicating that the model has improved by including higher resolution data.

Supplementary Fig. 1

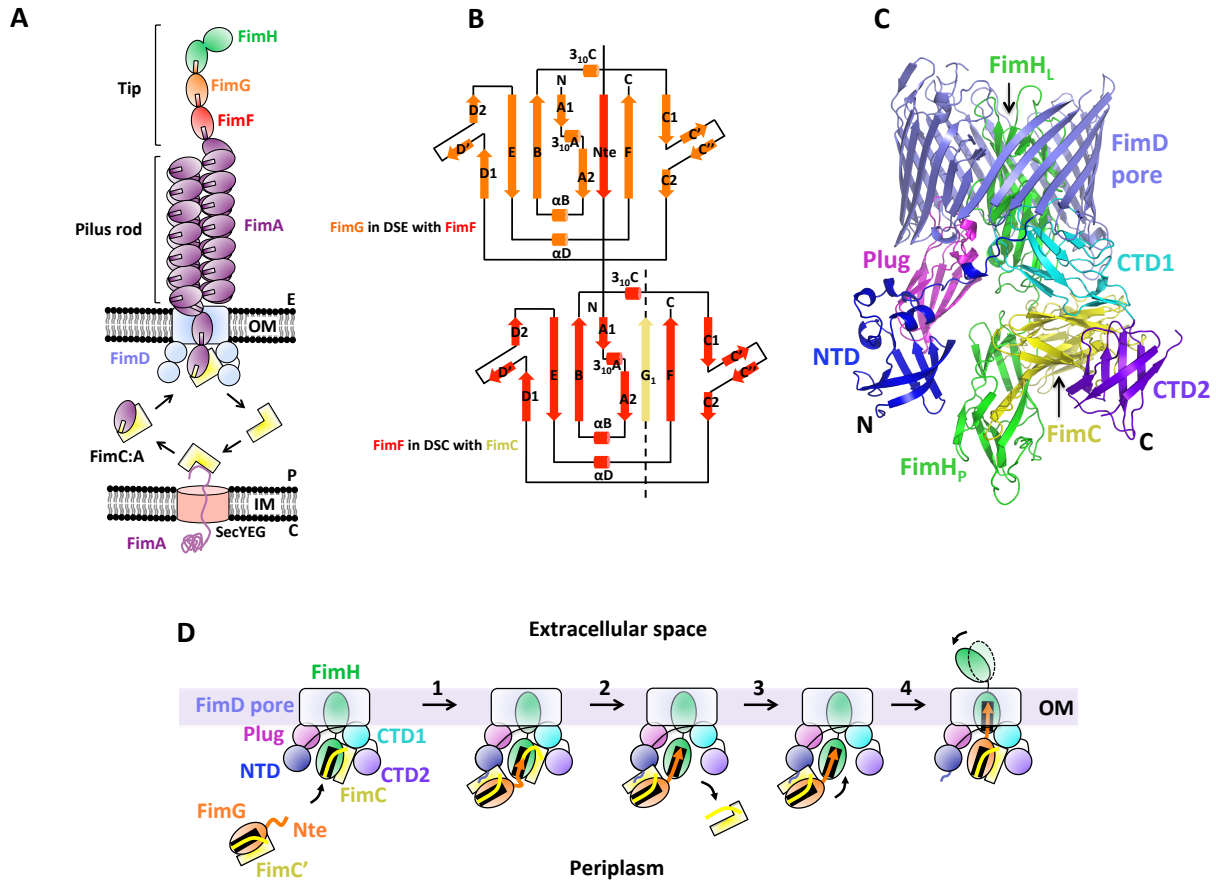

Introduction to type 1 pilus structure and assembly. A) Schematic diagram of a type 1 pilus. FimH, the tip adhesin, followed by FimG and FimF, form the tip fibrillum part of the pilus; a large polymer of FimA forms the rod. The pilus is anchored to the usher FimD, an outer membrane protein that serves as an assembly platform and a secretion machinery. The SecYEG translocon is used to transport subunits through the inner membrane and release them in the periplasm where they form binary complexes with the chaperone FimC. Color-coding of pilus subunit is green, orange, red and magenta for FimH, FimG, FimF, and FimA, respectively. The FimD usher is in light blue and the chaperone FimC is in yellow. The SecYEG translocon is colored light red. E, OM, P, IM, and C indicate the extracellular milieu, the outer membrane, the periplasm, the inner membrane and the cytoplasm, respectively. **B)**

Donor-strand complementation (DSC) and donor-strand exchange (DSE). All pilus subunits exhibit a C-terminally truncated Ig-fold lacking strand G, the last strand in the fold. As a result, a large groove is created at the subunit's surface where strand G should be. The chaperone FimC donates *in trans* one of its own strands to complement the subunit's fold in a process termed "donor-strand complementation (DSC)". During pilus biogenesis at the usher, the chaperone's strand is exchanged with the N-terminal extension peptide of the subunit next in assembly in a process termed "donor-strand exchange (DSE)". In this panel, topology diagrams for FimG in DSE with FimF (i.e. the Nte of FimF inserted into the groove of FimG) itself in DSC with FimC (i.e. the G1 strand of the FimC chaperone inserted into the groove of FimF) are shown. Color coding of pilus subunits and chaperone are as in A. **C) Structure of the FimD:FimC:FimH complex.** Color coding and representation of the various domains of FimD and of the various other proteins is as in main Fig. 1A. **D) Model of the usher-mediated subunit incorporation cycle.** The first schematic diagram at left shows the structure in panel C with the same color-coding of proteins and domains. The subsequent steps are structurally unknown. The groove in all subunits is highlighted black. The first step is the recruitment of FimC:FimG to the FimD NTD. This positions FimG and FimH for donor-strand exchange (DSE) and release of the chaperone on FimH (steps 2 and 3). Finally, in step 4, transfer of the nascent pilus from the NTD to the CTDs occurs concomitantly to translocation of the nascent pilus through the pore.

Supplementary Fig. 2

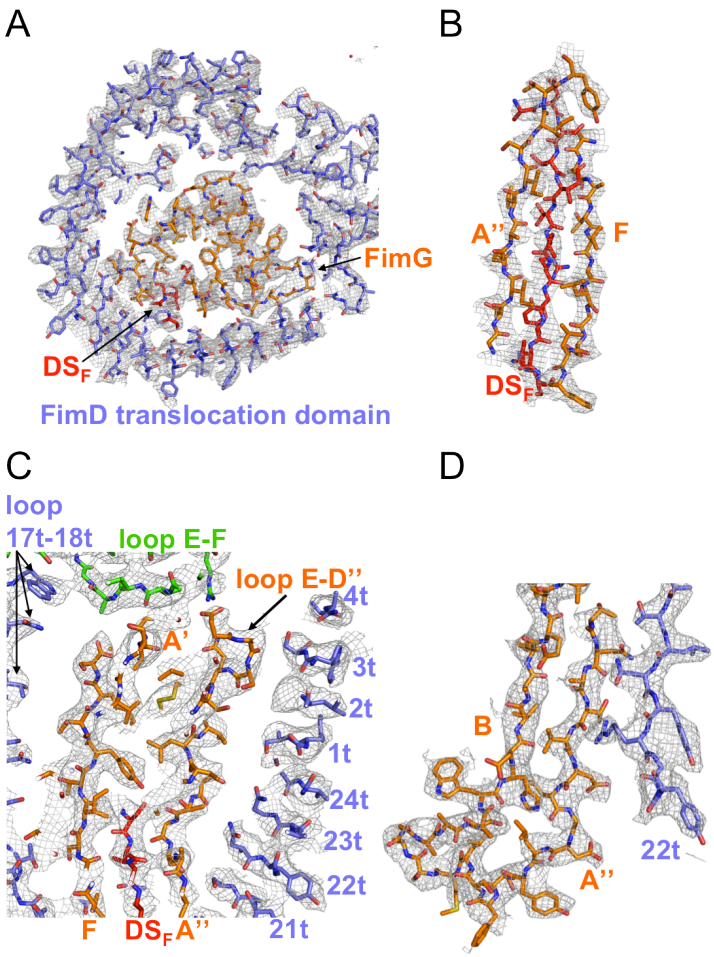

Averaged kicked electron density map of representative regions of the electron density. An averaged kicked electron density map [2] was created by PHENIX MAPS (version 1.8-1069). The electron density map was calculated in a resolution range of 83.67-3.80 Å, B-factor sharpened and contoured at 1.2 σ. The refined FimD:FimC:FimF:FimG:FimH model is shown in stick representation. Subunits are labeled according to nomenclatures of Choudhury et al., Puorger et al. and Phan et al. [3-5]. **A)** Lateral cross section of the entire usher translocation domain. The FimD pore domain, FimG and the donor strand of FimF (DS_F) are colored slate, orange and red, respectively. **B)** β-sheet consisting of donor strand of FimF (DS_F; red) and β-strands A'' and F of FimG (orange). **C)** Cross section along the vertical axis of the usher

translocation domain. Donor strand of FimF (DS_F), secondary structure elements of FimH, FimG and FimD translocation domain are colored red, green, orange and slate, respectively. **D)** β-strands A'' and B of FimG (orange) next to β-strand 22t of the FimD pore domain (slate).

Supplementary Fig. 3

A

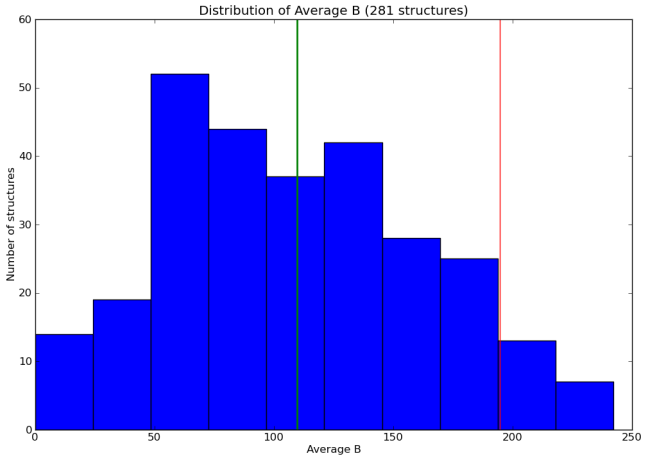

B

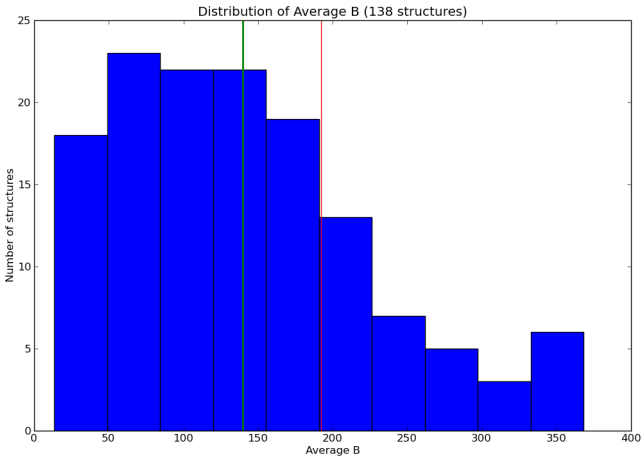

C

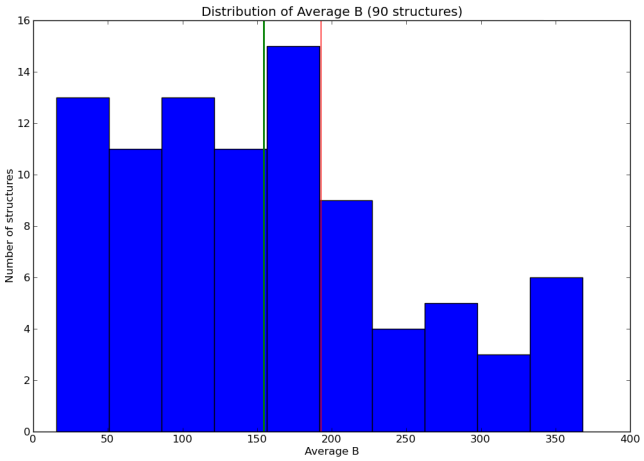

Comparison of mean B values between the FimD:FimC:FimF:FimG:FimH structures and structures deposited in the Protein Data Bank.

The histograms of the distribution of the mean B values among PDB entries solved at 3.8 Å, 4.1 Å and 4.3 Å resolutions are reported in panels A, B, C, respectively. The number of structures is indicated on the Y-axis. The mean B-factor of all PDB entries and that of the FimD:FimC:FimF:FimG:FimH structure at the stated resolution are indicated by a green and red line, respectively. The comparisons show that the mean B value of the FimD:FimC:FimF:FimG:FimH structure lies within the B value range of structures found in the PDB at every chosen resolution limit.

Supplementary Fig. 4

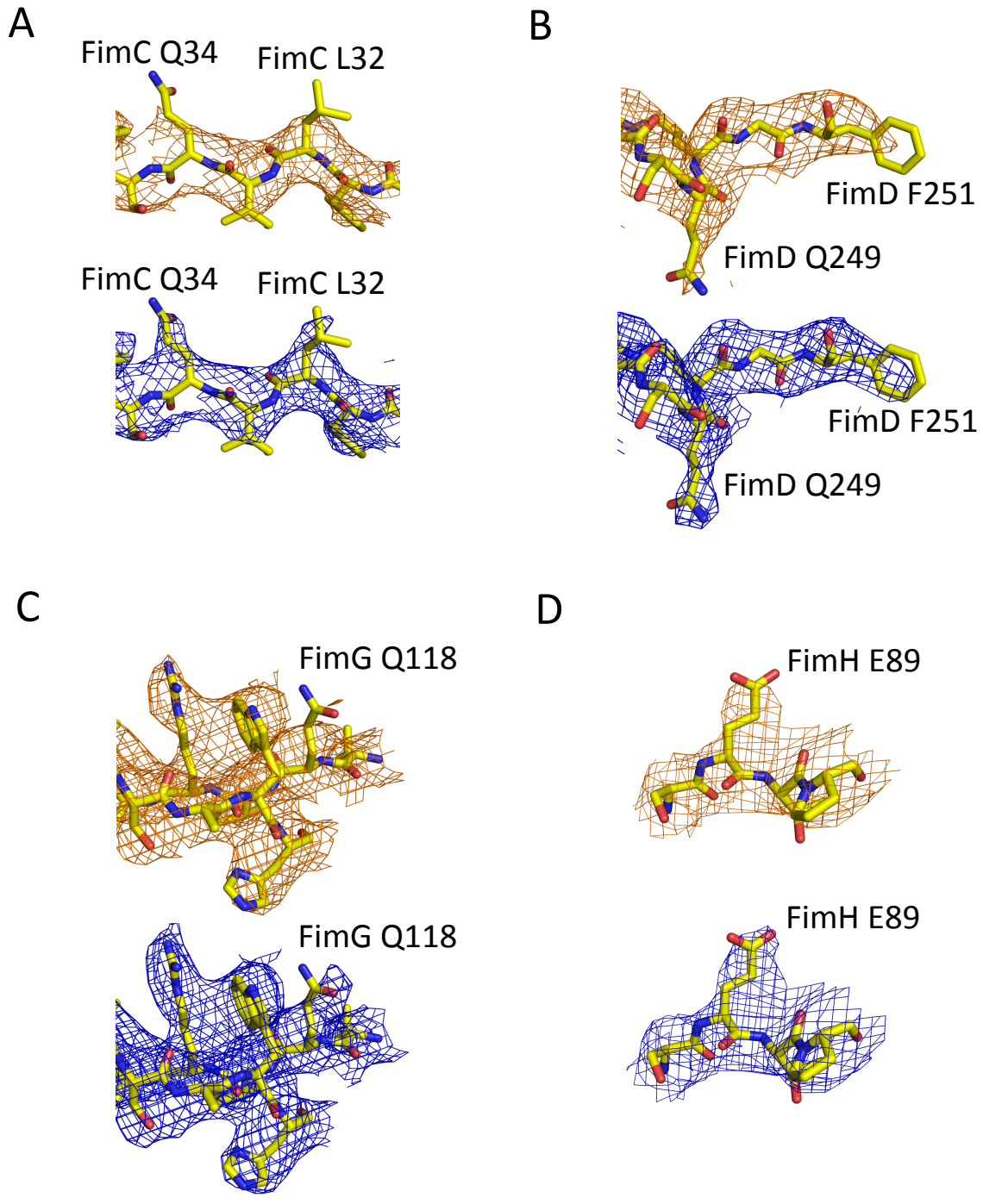

Comparison of electron density maps at 3.8 Å (blue) and 4.1 Å (orange) resolution. Averaged kicked, B-factor sharpened, maps are contoured at 1σ level. Four regions are

detailed in each of the proteins forming the FimD:FimC:FimF:FimG:FimH complex. As can be seen, extending the resolution to 3.8 Å results in an improvement of the electron density for side chains, thereby improving their positioning in the model.

Supplementary Fig. 5

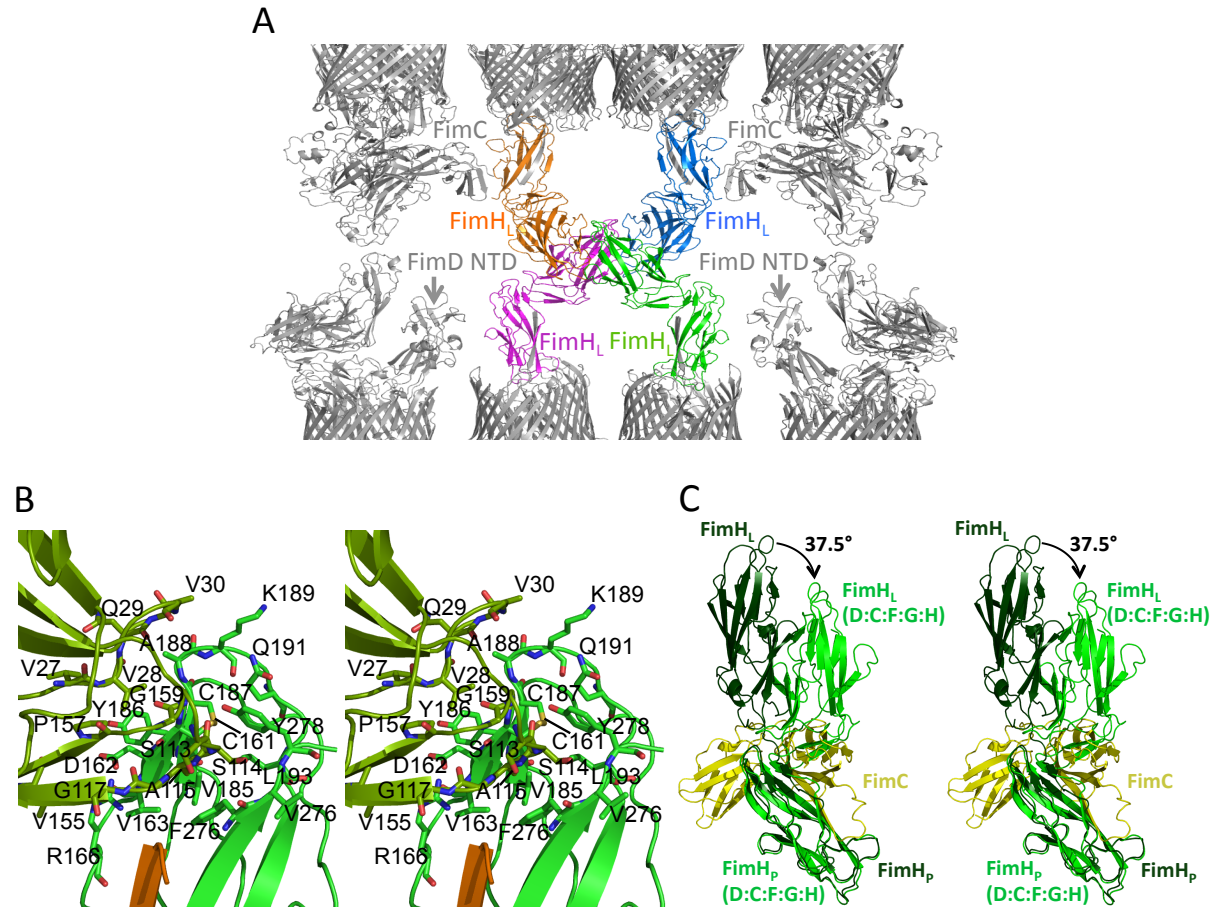

Crystal packing interface involving the FimH lectin domain (A); details of the FimH$_L$/FimH$_P$ interface in the FimD:FimC:FimF:FimG:FimH complex (B); and mechanism of FimH$_L$/FimH$_P$ interface formation (C).

A) Crystal packing interface involving the FimH$_L$ domain. Four symmetry-related FimH lectin domains come together in the crystal. This occurs through two contact surface areas, one of 485 Å^2 (between the structures in orange and magenta or between the structures in blue and green) and the other of 44 Å^2 (between the structures in orange and blue and between the structures in magenta and green). Janin and Rodier (1995)[6] in a survey of crystal-packing interfaces remark that most crystal-packing interfaces are weak unless they exceed 1500 Å^2. We also note that the average B-factor value for the FimH lectin domain is similar to that of

the entire structure. We conclude that although crystal packing might have some stabilizing effects resulting in an average B-factor value similar to that of the entire structure, these effects are likely too small to impose a conformational change on FimH.

B) Details of the $FimH_L/FimH_P$ interface in the FimD:FimC:FimF:FimG:FimH complex. Residues involved in interactions are shown in stick representations with C, O, N and S atoms colour-coded in green, red, blue and yellow, respectively. $FimH_L$ and $FimH_P$ are in ribbon representation colour-coded in dark and light green, respectively. The interface is 462 $Å^2$ large and is contributed by no fewer than 25 residues. This interface might not be apparently larger than the crystal packing interface of 485 $Å^2$ mentioned above, but will be substantially stronger because it involves two adjacent domains in the same protein i.e. two domains linked covalently. This increases considerably the local concentration of the two interface partners and massively displaces the equilibrium towards interface formation. It is therefore clear that the $FimH_L/FimH_P$ interface is much more energetically favored than the $FimH_L/FimH_L$ interface we see between symmetry-related molecules and thus, this is the dominant interface imposing the conformational change. We can therefore conclude that the conformational change which we observed in FimH before and after transport is not caused by crystal-packing forces.

C) Mechanism of $FimH_L/FimH_P$ interface formation. The structure of FimC:FimH (yellow and dark green) in the FimD:FimC:FimH complex was here superimposed with the structure of FimH (light green) in the FimD:FimC:FimF:FimG:FimH complex using $FimH_P$ for the superposition exercise. All structures are in ribbon representation. In the FimD:FimC:FimH structure, the interface between $FimH_L$ and $FimH_P$ is only 210 $Å^2$, i.e. much smaller than the interface observed between the two domains in the FimD:FimC:FimF:FimG:FimH structure (462 $Å^2$). The superposition shown here clearly demonstrates that FimC prevents the FimH domains from closing in i.e. maintains FimH in an open conformation. We conclude that, prior to transport, FimC imposes a more open conformation on FimH; however, post-transport, FimH being no longer bound to FimC, the two domains of FimH can close in and form the interface seen in the FimD:FimC:FimF:FimG:FimH complex.

Supplementary Fig. 6

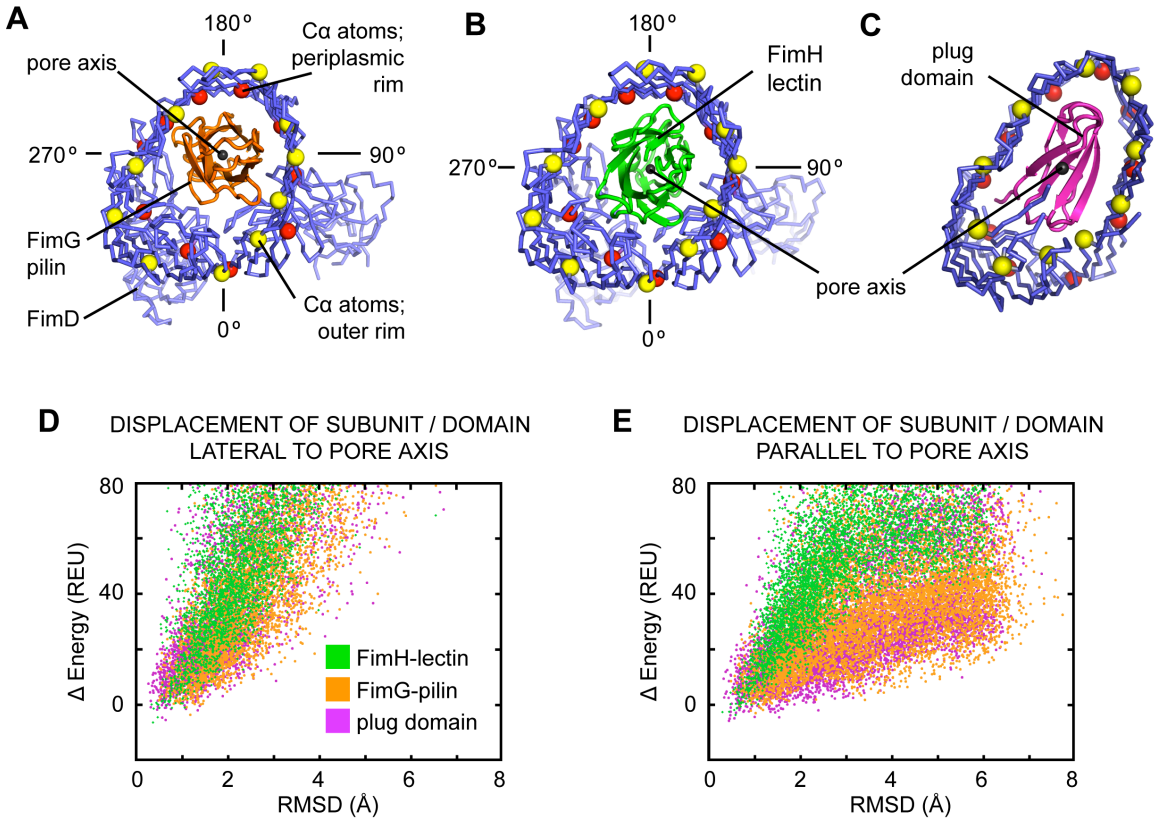

Lateral translation of the translocating substrate within the usher pore causes a steep increase in calculated potential energy.

A) A pore axis is defined as passing through the geometric centre of the translocating subunit and as parallel to the vector between the midpoints of Cα atoms lining the extracellular (yellow spheres: H160, S184, H200, L218, Q370, S413, Q505, D546, M586, S618, Q647) and periplasmic (red spheres: L142, R207, S240, L322, L422, Y499, T531, S575, T595, N634) rims of the usher barrel. Extraneous subunits outside the pore were removed, such that only FimD (slate ribbon) and the transported cargo domains $FimH_L$ (not shown) or FimG (orange cartoon; complete with the complementing Nte of FimF) from the respective crystal structures were considered. This view is from outside the bacterium and straight down the pore axis. Angular directions around the FimD pore axis are set with FimD-Asp208 at 0º and counterclockwise is positive.

B) $FimH_L$ (green cartoon) inside FimD (slate ribbon) from crystal structure FimD:FimC:FimH, viewed as in panel A.

C) Crystal structure of apo-FimD (slate ribbon; PDB 3OHN) viewed from outside the bacterium, looking down the pore axis. The pore axis is defined as described for FimD:FimC:FimH or FimD:FimC:FimF:FimG:FimH above, except that the chosen Cα atoms representing the extracellular and periplasmic rims of apo-FimD are different due to the large conformational differences between these two sets of structures. The pore axis passes through the geometric centre of the plug domain (magenta cartoon; residues 254-320) and parallel to a vector between the midpoints of regularly spaced Cα atoms lining the extracellular (yellow spheres: N149, S184, I201, N232, T447, A477, H504, Q547, A611, D644) and periplasmic rims (red spheres: L142, R207, Q324, Y331, N419, T489, A524, S575, D599, V652).

D and E) FimG-pilin (orange), $FimH_L$ (green) and the plug domain (magenta) were randomly rotated within ± 8º about their geometric centres and randomly translated up to 6 Å perpendicular/lateral **(D)** or parallel **(E:** the outline of the lowest energy conformations is shown in main Fig. 3C) to the pore axis. The perturbed structures were minimized and the calculated energies plotted against the rmsd to the respective minimized crystal structures. 8000 total perturbations for each. The plug domain and FimG have, compared to $FimH_L$, low energy barriers for displacement along the pore axis, whereas there is a steep energy increase for lateral perturbations of any of the subunits/domains.

Supplementary Fig. 7

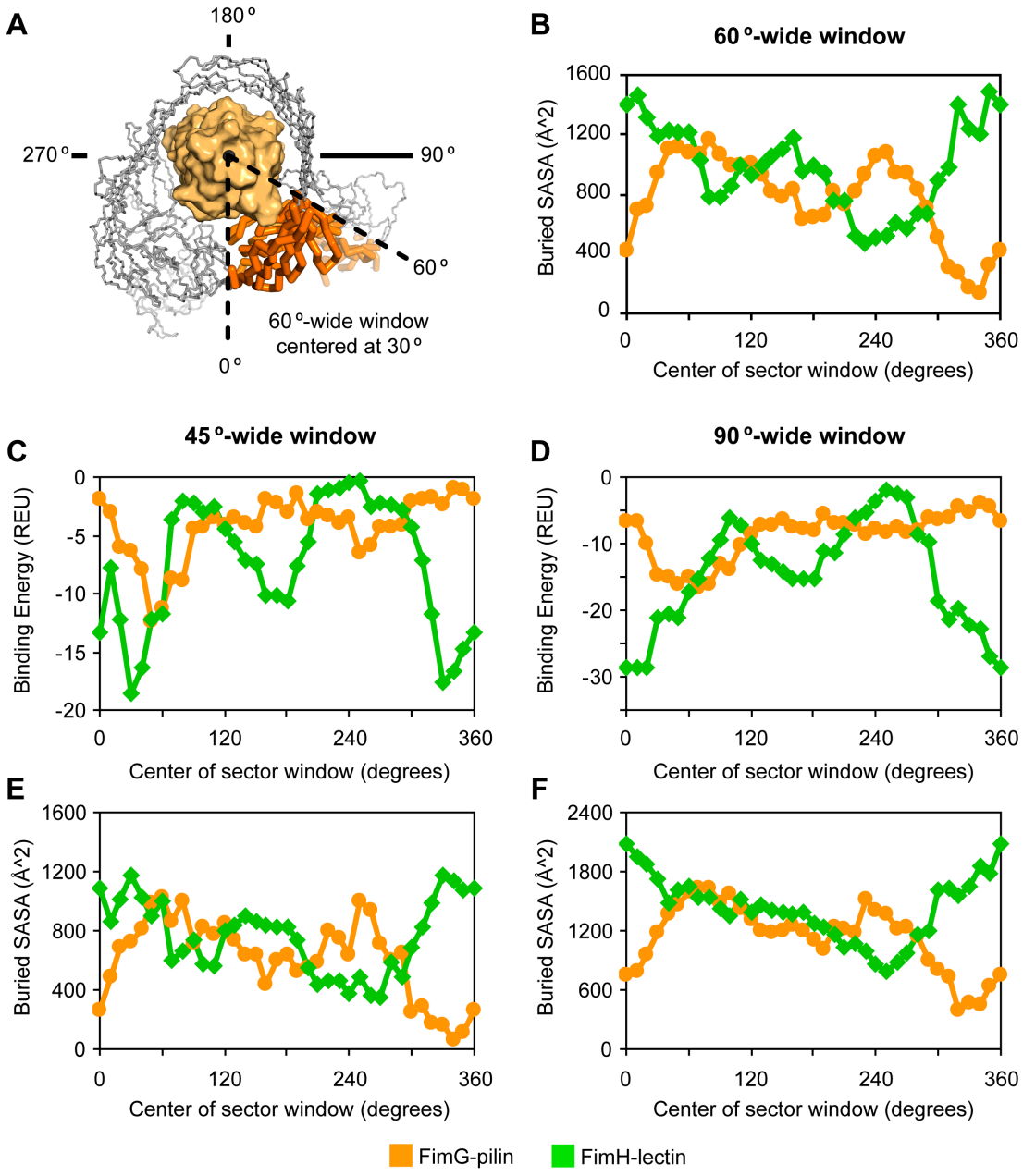

Patterns in calculated binding energies around the FimD lumen are conserved with different width windows.

FimG (plus Nte of FimF) inside the FimD pore is orange, $FimH_L$ inside the pore is green.

A) Top view looking down the pore axis of FimG (pale orange surface) inside the FimD (thin

grey ribbon) lumen. For illustrative purposes, a representative window from 0-60º is shown by dashed lines. The region of FimD included in this example window is in thick orange ribbon. 0º is set as the direction from the pore axis to the Cα atom of FimD-Asp208.

B) Physical intimacy of interface contacts measured by buried solvent accessible surface area (SASA) as a 60º-sector window emanating from the pore axis is rotated around the respective structures.

C and D) Calculated binding energy to FimD within sector-shaped windows of 45º and 90º widths. The approximation of binding energy peaks for FimG correlating to nearby troughs for $FimH_L$, and vice versa, is still observed at the different window sizes. Further, binding energy troughs are approximately 180º apart. The crystal structures were relaxed in the Rosetta force field heavily constrained by the crystallographic electron density prior to analysis (see Methods).

E and F) Buried SASA between the FimD sector and the translocating substrate, as in panel B but for different sector widths. Binding energy troughs partially correlate with increased physical intimacy as measured by peaks in buried SASA.

Supplementary Fig. 8

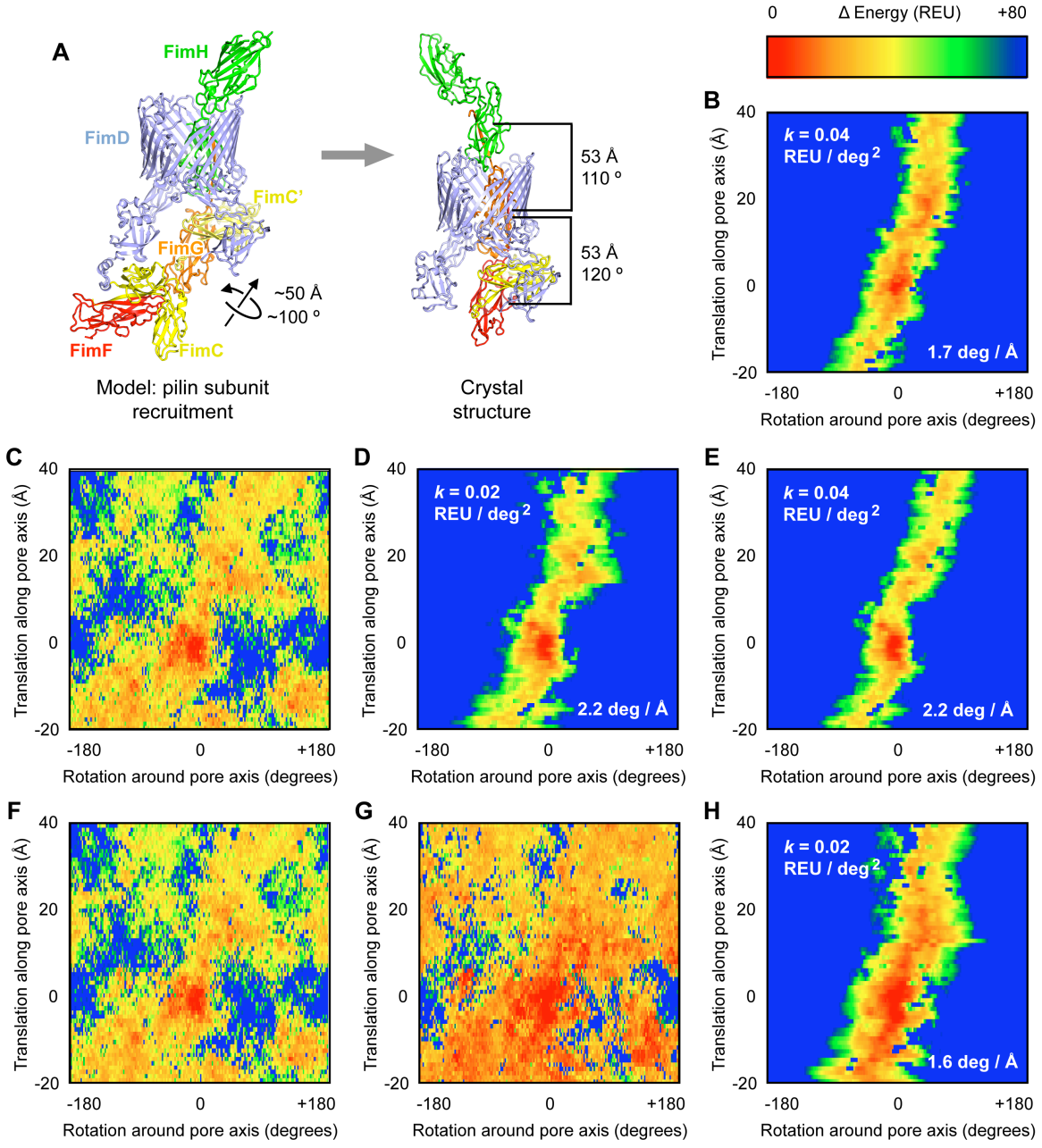

Features of the computed energy landscape for FimG entry-exit in the usher pore are resilient to changes in initial structure preparation, fold tree connectivity and spring constant choice.

A) On the left is a model of FimD:FimC':FimG:FimH recruiting a FimC:FimF subunit to the FimD NTD, which following DSE, release of chaperone FimC' and translocation of the growing pilus from the NTD to CTDs, is resolved to form crystal structure FimD:FimC:FimF:FimG:FimH. Transformations between the domains in the growing pilus tip are indicated.

B) A trajectory was traced through the energy landscape of main Fig. 4A by applying a torsional spring potential term at each 1 Å FimG translational step to ensure connectivity along conformational space. The trajectory must travel through the native state (0 Å translation, 0º rotation) and follows the lowest energy path. Here, a torsional spring constant twice that in main Fig. 4B further limits the extent to which FimG fluctuates around its rotational axis and imposes tighter connectivity. A counterclockwise twist as FimG translocates is still observed in the trajectory, though the extent of rotation is diminished from 3.0 to 1.7 degrees per angstrom.

C) The previously described energy landscapes were derived beginning with the crystal structure refined to 3.8 Å resolution based on $CC_{1/2}$ = 0.18 at the highest resolution shell (3.9 - 3.8 Å). Here, the calculated energy landscape is presented beginning with the crystal structure refined to 4.1 Å resolution based on traditional measures of diffraction data quality (see Supplementary Table 1).

D) Applying a torsional spring potential term to the energy landscape in panel C, with spring constant k = 0.02 Rosetta Energy Units (REU) per degree^2, predicts a counterclockwise rotation of 2.2º/Å.

E) As in (D), but doubling the torsional spring constant.

F) Rosetta uses atom tree and fold tree representations to store structural information, with jump connections in the fold tree between different chains of a multi-subunit complex [7]. Rigid-body minimization occurs over the jump/rigid-body degree of freedom. In main Fig. 4 and panel C, the fold tree jump was defined between the C-terminus of FimD and the N-terminus of FimF-Nte complementing the FimG-pilin domain. Here, an almost identical energy landscape is presented to that in panel C in which an alternative jump connection was defined between the FimG C-terminus and the FimD N-terminus.

G) In previous panels, the starting refined crystal structure was pre-minimized using Rosetta's full atom score12 prior to rotating and translating FimG within the usher lumen. This is

consistent with how the perturbed structures are themselves then minimized. Here, the refined crystal structure was instead first relaxed in Rosetta's force field modified by strong constraints to the crystallographic electron density map, followed by rotating/translating FimG and minimizing the perturbed structures as before.

H) Mapping the trajectory through the energy landscape of panel G.

Supplementary Fig. 9

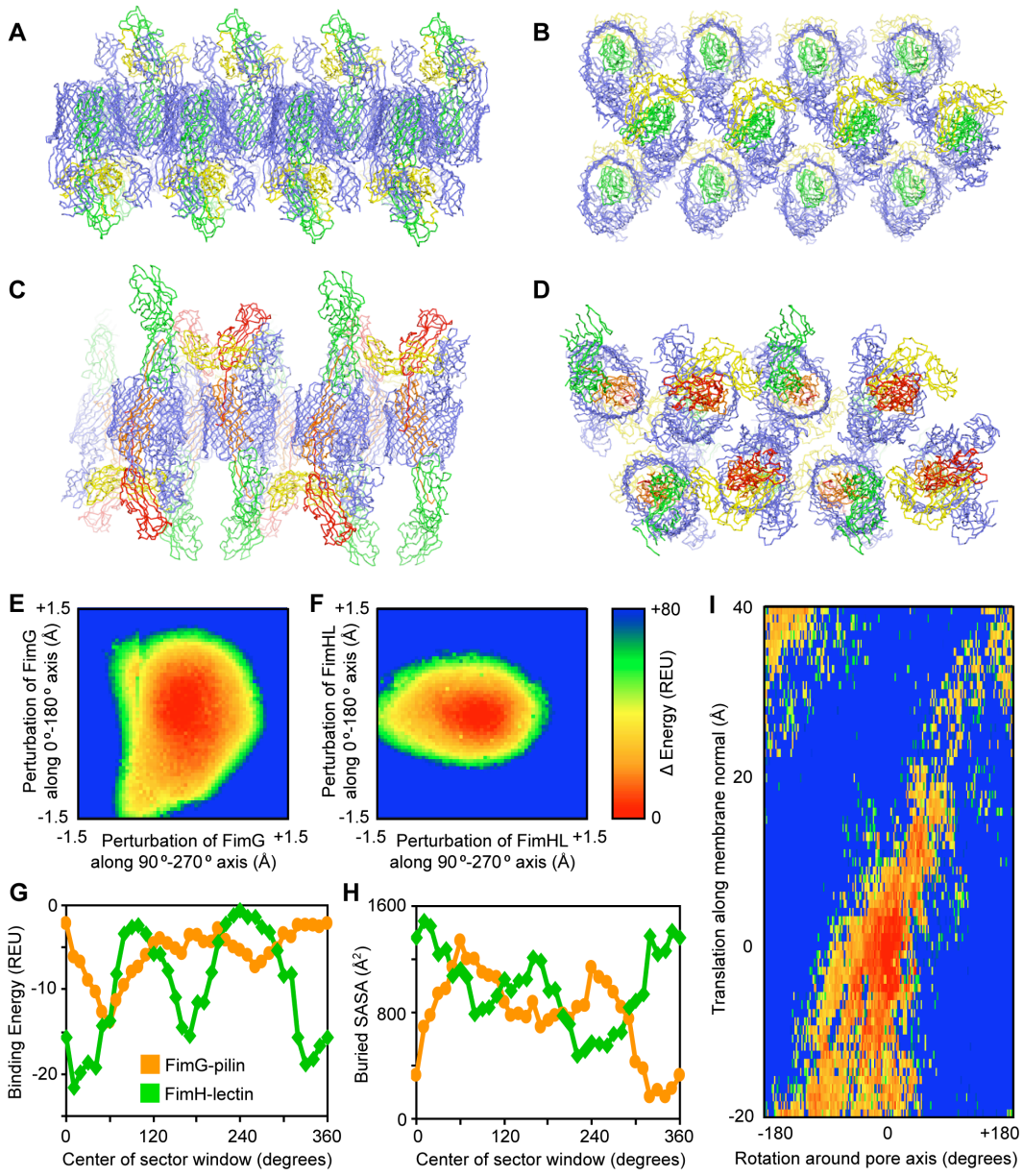

Results of computational analyses are reproducible using an alternatively defined pore axis based on the membrane-like arrangement of FimD proteins within the crystal lattices.

The membrane-spanning, hydrophobic β-barrel of FimD packs in the crystal lattice as membrane-like layers. Shown are single layers viewed from the side **(A and C)** and from

above **(B and D)** of FimD:FimC:FimH **(A and B)** and FimD:FimC:FimF:FimG:FimH **(C and D)** in their respective crystal lattices. Apo-FimD (PDB 3OHN) similarly arranges into membrane-like layers propagated through the crystal (not shown). As an alternative to the pore axes described in the main text, we repeated some of the important analyses using instead the normal to the membrane layers seen in the crystal packing (passing through the geometric centre of the substrate). FimD, slate; FimC, yellow; FimF, red; FimG, orange; and FimH, green.

E) FimG is translated laterally/perpendicular to the membrane normal within the FimD lumen by small increments, and side chain rotamers are repacked-minimized while the shifted backbones are held fixed. Energy is plotted as a heat map against the lateral translation, showing a sharp energy well towards the native conformation.

F) As in panel E, except $FimH_L$ is inside FimD from its respective crystal structure.

G) Interface binding energy within a 60º-wide sector window that emanates from and is rotated around the membrane normal.

H) Physical intimacy of interface contacts measured by buried solvent accessible surface area (SASA) within a 60º-wide sector window rotated around the membrane normal.

I) FimG within the FimD lumen is rotated by a full 360º in 2º increments around the membrane normal, and translated along the membrane normal 40 Å out to the extracellular space and 20 Å in towards the periplasm in 1 Å steps. At each sampled FimG rotation-translation, the structure is minimized and the energy plotted. Whilst the energies are higher than those calculated for the pore axis defined in the main text – and therefore less likely to represent the true path FimG takes during transport – there remains a clear lower energy preference for a counterclockwise rotation of FimG during translocation.

Supplementary Fig. 10

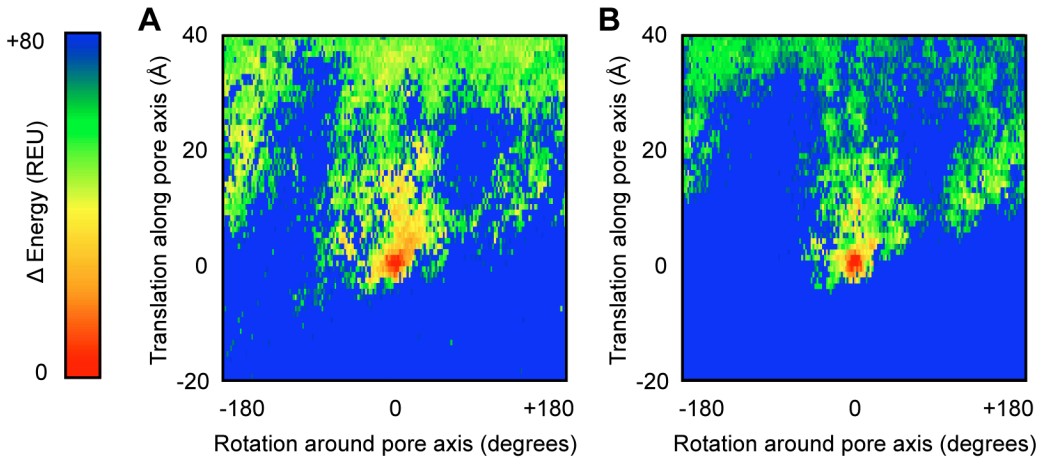

$FimH_L$ entry-exit energy landscape.

A) Energy landscape as $FimH_L$ is rotated-translated along its pore axis (see description for main Fig. 4) within the FimD lumen from its native crystal structure FimD:FimC:FimH. Negative translations of $FimH_L$ back towards the periplasm cause an abrupt and large increase in energy, easily rationalized from the crystal structure showing contacts from the plug and CTD1 partially blocking $FimH_L$'s escape back in to the periplasm. Hence the initiating conformational changes that expel the plug domain from the usher lumen and insert the FimH lectin domain inside will need to be at least in part undone for $FimH_L$ to reverse-translate back. When $FimH_L$ is translated outwards, the energies on the calculated landscape again increase more steeply than observed for FimG, consistent with $FimH_L$ being a putative tighter binder. There is no clear low energy path for $FimH_L$ exit.

B) As in A, except $FimH_L$ is now translated along and rotated around the membrane normal observed in the crystal lattice. Again, no clear low energy exit path is observed.

Supplementary Fig. 11

Command line and score term weights for relaxing the FimD:FimC:FimF:FimG:FimH and FimD:FimC:FimH crystal structures with electron density constraints.

```
./relax.static.linuxgccrelease -edensity::mapfile mapfile.ccp4 -
s structure.pdb -in:ignore_unrecognized_res -database
rosetta_database_directory -nstruct 50 -
relax::minimize_bond_angles -relax::minimize_bond_lengths -
default_max_cycles 200 -relax::min_type lbfgs_armijo_nonmonotone
-relax::jump_move true -score:weights weights_file -
bonded_params 400 400 100 10 -relax:default_repeats 2 -
relax:cartesian -edensity::mapreso 5.0 -edensity::grid_spacing
2.0 -edensity::realign min -mute core.conformation core.chemical
core.optimization -chemical:exclude_patches LowerDNA  UpperDNA
Cterm_amidation SpecialRotamer  VirtualBB ShoveBB
VirtualDNAPhosphate VirtualNTerm CTermConnect sc_orbitals
pro_hydroxylated_case1 pro_hydroxylated_case2 ser_phosphorylated
thr_phosphorylated  tyr_phosphorylated tyr_sulfated
lys_dimethylated lys_monomethylated  lys_trimethylated
lys_acetylated glu_carboxylated cys_acetylated tyr_diiodinated
N_acetylated C_methylamidated MethylatedProteinCterm

METHOD_WEIGHTS ref  0.16 1.7 -0.67 -0.81 0.63 -0.17 0.56 0.24 -
0.65 -0.1 -0.34 -0.89 0.02 -0.97 -0.98 -0.37 -0.27 0.29 0.91
0.51
fa_atr 0.8
fa_rep 0.44
fa_sol 0.65
fa_intra_rep 0.004
fa_pair 0.49
fa_plane 0
fa_dun 0.56
ref 1
hbond_lr_bb 1.17
hbond_sr_bb 0.585
hbond_bb_sc 1.17
hbond_sc 1.1
p_aa_pp 0.32
dslf_ss_dst 0.5
dslf_cs_ang 2
dslf_ss_dih 5
dslf_ca_dih 5
pro_close 1.0
rama 0.2
omega 0.5
atom_pair_constraint 0.0
coordinate_constraint 0.0
cart_bonded 0.5
elec_dens_fast 8.0
```

Supplementary Fig. 12

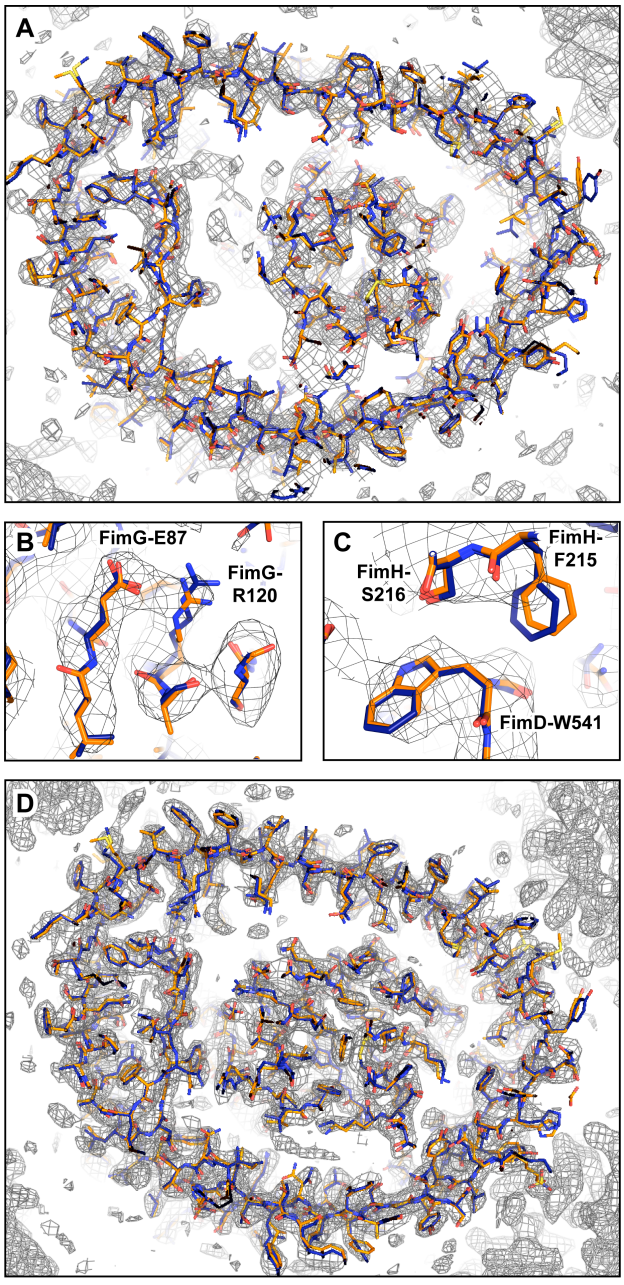

Fit of Rosetta-relaxed structures to the crystallographic model coordinates and electron density maps. In all panels the refined crystal structure is dark blue, the Rosetta-relaxed structure is orange, and the electron density at 1 σ is grey mesh.

A) Slice through FimD:FimC:FimF:FimG:FimH, looking at a cross-section through the usher

pore with FimG inside.

B-C) Close-up views of individual residues of FimD:FimC:FimF:FimG:FimH, demonstrating that the Rosetta-relaxed structure is consistent with the electron density.

D) Slice through the higher resolution FimD:FimC:FimH structure, in a similar orientation to panel A, with FimH inside the usher pore.

Supplementary Fig. 13

Command line and Rosettascripts protocol for determining binding energies and buried solvent accessible surface areas of FimD sectors bound to either FimH-lectin or FimG.

```
./rosetta_scripts.static.linuxiccrelease -database
minirosetta_database/ -parser:protocol
rosettascripts_protocol.xml -l input_structures.list -nstruct 1
-jd2:ntrials 5 -ignore_unrecognized_res -ex1 -ex2 -
extrachi_cutoff 5 -no_his_his_pairE -use_input_sc


<ROSETTASCRIPTS>
<SCOREFXNS>
</SCOREFXNS>
<FILTERS>
        <Ddg name=ddg scorefxn=score12 threshold=100
repack=false repeats=1 confidence=0/>
        <Sasa name=sasa threshold=0/>
</FILTERS>
<MOVERS>
</MOVERS>
<PROTOCOLS>
        <Add filter_name=ddg/>
        <Add filter_name=sasa/>
</PROTOCOLS>
</ROSETTASCRIPTS>
```

Supplementary Fig. 14

Command line and Rosettascripts protocol for minimizing perturbed structures, in which the subunit occupying the pore (FimH-lectin, FimG, or the plug domain) was first randomly rotated and randomly translated parallel or lateral to the pore axis using the convpdb.pl application in the MMTSB suite [8].

```
./rosetta_scripts.static.linuxiccrelease -database
minirosetta_database/ -parser:protocol
rosettascripts_protocol.xml -l input_structures.list -nstruct 1
-jd2:ntrials 5 -ignore_unrecognized_res -ex1 -ex2 -
extrachi_cutoff 5 -no_his_his_pairE -use_input_sc -
in:file:native minimized_native_structure.pdb -out::file::silent
silent.out -out::file::silent_struct_type binary -
out:file:scorefile score.sc -mute all
```

```
<ROSETTASCRIPTS>
<SCOREFXNS>
</SCOREFXNS>
<FILTERS>
        <Ddg name=ddg scorefxn=score12 threshold=100 repack=1
repeats=1 confidence=0/>
        <Rmsd name=rmsd chains="B" threshold=100 superimpose=0/>
</FILTERS>
<MOVERS>
        <MinMover name=min scorefxn=score12 chi=1 bb=1 jump=0,1
type=dfpmin_armijo_nonmonotone tolerance=0.01/>
        <Prepack name=ppk scorefxn=score12 jump_number=0/>
</MOVERS>
<PROTOCOLS>
        <Add mover_name=ppk/>
        <Add mover_name=min/>
        <Add filter_name=ddg/>
        <Add filter_name=rmsd/>
</PROTOCOLS>
</ROSETTASCRIPTS>
```

Supplementary Fig. 15

Command line and Rosettascripts protocol for fixed backbone minimization of structures in which the subunit occupying the FimD pore was first translated lateral to the pore axis along a finely-spaced grid using convpdb.pl from the MMTSB suite [8].

```
./rosetta_scripts.static.linuxiccrelease -database
minirosetta_database/ -parser:protocol
rosettascripts_protocol.xml -l input_structures.list -nstruct 1
-jd2:ntrials 5 -ignore_unrecognized_res -ex1 -ex2 -
extrachi_cutoff 5 -no_his_his_pairE -use_input_sc -
out::file::silent silent.out -out::file::silent_struct_type
binary -out:file:scorefile score.sc -mute all
```

```
<ROSETTASCRIPTS>
<SCOREFXNS>
</SCOREFXNS>
<FILTERS>
</FILTERS>
<MOVERS>
        <MinMover name=min scorefxn=score12 chi=1 bb=0
type=dfpmin_armijo_nonmonotone tolerance=0.01/>
        <Prepack name=ppk scorefxn=score12 jump_number=0/>
</MOVERS>
<PROTOCOLS>
        <Add mover_name=min/>
        <Add mover_name=ppk/>
        <Add mover_name=min/>
        <Add mover_name=ppk/>
        <Add mover_name=min/>
</PROTOCOLS>
</ROSETTASCRIPTS>
```

Supplementary Fig. 16

Command line and Rosettascripts protocol for minimization of structures in which FimH-lectin or FimG were translated by discrete 1 Å steps along and rotated by a full 360º in 2º steps around the pore axis. Translations and rotations were first made external to Rosetta software using the MMTSB suite.

```
./rosetta_scripts.static.linuxiccrelease -database
minirosetta_database/ -parser:protocol
rosettascripts_protocol.xml -l input_structures.list -nstruct 1
-jd2:ntrials 5 -ignore_unrecognized_res -ex1 -ex2 -
extrachi_cutoff 5 -no_his_his_pairE -use_input_sc -
out::file::silent silent.out -out::file::silent_struct_type
binary -out:file:scorefile score.sc -mute all
```

```
<ROSETTASCRIPTS>
<SCOREFXNS>
</SCOREFXNS>
<FILTERS>
        <Ddg name=ddg scorefxn=score12 threshold=100 repack=1
repeats=1 confidence=0/>
</FILTERS>
<MOVERS>
        <MinMover name=min scorefxn=score12 chi=1 bb=1 jump=0,1
type=dfpmin_armijo_nonmonotone tolerance=0.01/>
        <Prepack name=ppk scorefxn=score12 jump_number=0/>
</MOVERS>
<PROTOCOLS>
        <Add mover_name=ppk/>
        <Add mover_name=min/>
        <Add mover_name=ppk/>
        <Add mover_name=min/>
        <Add filter_name=ddg/>
</PROTOCOLS>
</ROSETTASCRIPTS>
```

Supplementary references

1 Karplus, P. A. & Diederichs, K. Linking crystallographic model and data quality. *Science* **336**, 1030-1033 (2012).

2 Praznikar, J., Afonine, P. V., Guncar, G., Adams, P. D. & Turk, D. Averaged kick maps: less noise, more signal... and probably less bias. *Acta Crystallogr D Biol Crystallogr* **65**, 921-931 (2009).

3 Choudhury, D. *et al*. X-ray structure of the FimC-FimH chaperone-adhesin complex from uropathogenic *Escherichia coli*. *Science* **285**, 1061-1066 (1999).

4 Phan, G. *et al*. Crystal structure of the FimD usher bound to its cognate FimC-FimH substrate. *Nature* **474**, 49-53 (2011).

5 Puorger, C. *et al*. Infinite kinetic stability against dissociation of supramolecular protein complexes through donor strand complementation. *Structure* **16**, 631-642 (2008).

6 Janin, J. & Rodier, F. Protein-protein interactions at crystal contacts. *Proteins* **23**, 580-587 (1995).

7 Wang, C., Bradley, P. & Baker, D. Protein-protein docking with backbone flexibility. *J Mol Biol* **373**, 503-519 (2007).

8 Feig, M., Karanicolas, J. & Brooks, C. L., 3rd. MMTSB Tool Set: enhanced sampling and multiscale modeling methods for applications in structural biology. *J Mol Graph Model* **22**, 377-395 (2004).